Supporting Information

Tuning doping and surface functionalization of columnar oxide films for volatile organic compounds sensing: Experiments and theory

Vasile Postica,[a] Alexander Vahl,[b] Julian Strobel,[c] David Santos-Carballal,[d,ⱶ] Oleg Lupan,[a,e,†] Abdelaziz Cadi-Essadek,[d] Nora H. de Leeuw,[d,f,‡] Fabian Schütt,[e] Oleksandr Polonskyi,[b] Thomas Strunskus,[b] Martina Baum,[e] Lorenz Kienle,[c,ꟻ] Rainer Adelung,[e,˥] Franz Faupel[b,꜔]

a. *Department of Microelectronics and Biomedical Engineering, Center Nanotechnology and Nanosensors, Technical University of Moldova, 168 Stefan cel Mare Av., MD-2004 Chisinau, Republic of Moldova.*
b. *Chair for Multicomponent Materials, Institute for Materials Science, Kiel University, Kaiserstr. 2, D-24143, Kiel, Germany.*
c. *Synthesis and Real Structure, Institute for Materials Science, Kiel University, Kaiser str. 2, D-24143, Kiel, Germany.*
d. *School of Chemistry, Cardiff University, Main Building, Park Place, Cardiff CF10 3AT, United Kingdom.*
e. *Functional Nanomaterials, Institute for Materials Science, Faculty of Engineering, Kiel University, Kaiserstr. 2, D-24143, Kiel, Germany*
f. *Department of Earth Sciences, Utrecht University, Princetonplein 8A, 3584 CB Utrecht, The Netherlands.*

Received ZZZ, revised ZZZ, accepted ZZZ
Published online ZZZ (Dates will be provided by the publisher.)

† Corresponding author: e-mail ollu@tf.uni-kiel.de oleg.lupan@mib.utm.md lupanoleg@yahoo.com
ⱶ e-mail SantosCarballalD@Cardiff.ac.uk
‡ e-mail deLeeuwN@cardiff.ac.uk, n.h.deleeuw@uu.nl
ꟻ e-mail lk@tf.uni-kiel.de
˥ e-mail ra@tf.uni-kiel.de
꜔ e-mail ff@tf.uni-kiel.de

XPS investigation on highly doped ZnO:Fe10× thin film

A ZnO:Fe thin film with a higher iron doping concentration (Zno:Fe10×), increased to ten times the normal concentration was investigated by XPS. The corresponding spectra are shown **Figure S1**. In the overview spectrum, the elements Zn, Fe, O and C are detected. The presence of C originates in surface contamination by atmospheric organic compounds and the respective C-1s line is used for charge referencing as aliphatic C-1s at 285 eV. In case of the highly doped ZnO:Fe10x thin film, the characteristic iron lines Fe-$2p_{3/2}$ and Fe-$2p_{1/2}$ (**Figure S1b**) are located at 710.6 eV and 724.0 eV respectively, resulting in a peak spreading of 13.4 eV. The observed peak positions, the peak spreading as well as the peak shape with the satellites at higher binding energies correspond well to fully oxidized Fe_2O_3.

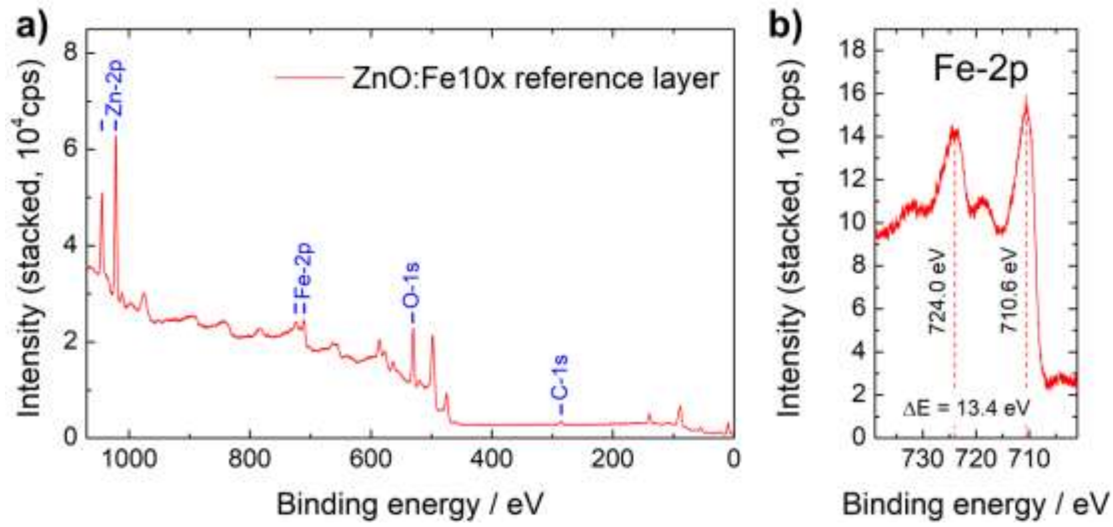

Figure S1. XPS spectra of a ZnO:Fe columnar thin film with increased iron doping concentration (10 times the reference concentration); a) overview spectrum; b) high resolution spectrum of Fe-2p lines.

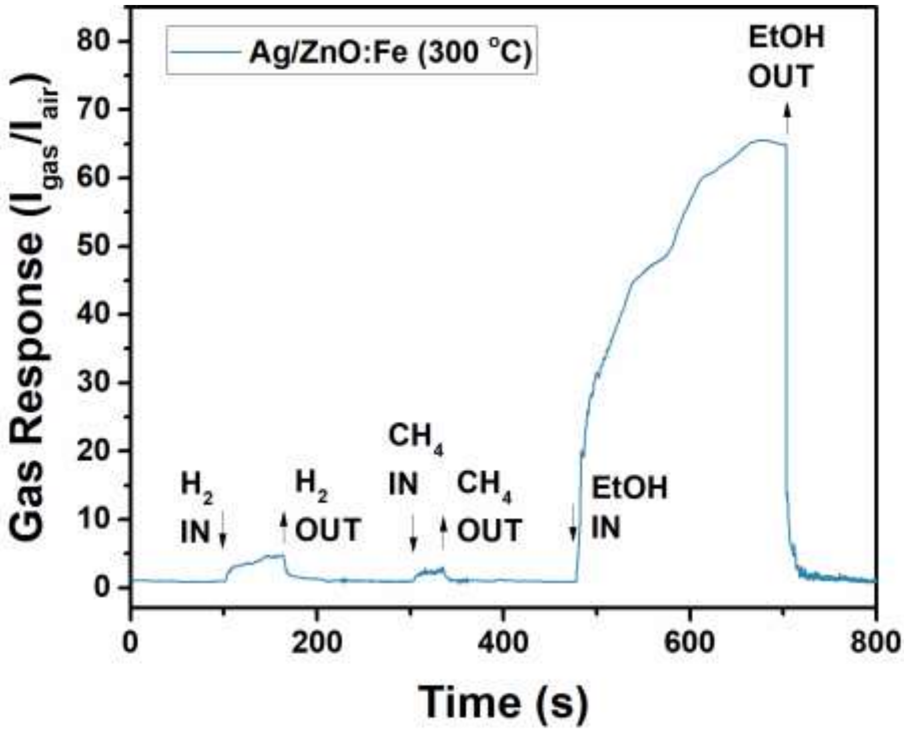

Figure S2. The gas response to H_2 (1000 ppm), CH_4 (1000 ppm) and ethanol vapors (20 ppm) at 300 ºC for Ag/ZnO:Fe nanostructured films.

TEM investigations of AgO/Ag on ZnO columnar structures

Ag NPs are only visible in HAADF contrast. They are invisible in TEM bright field mode; no high resolution micrographs could be recorded because of too high sample thickness.

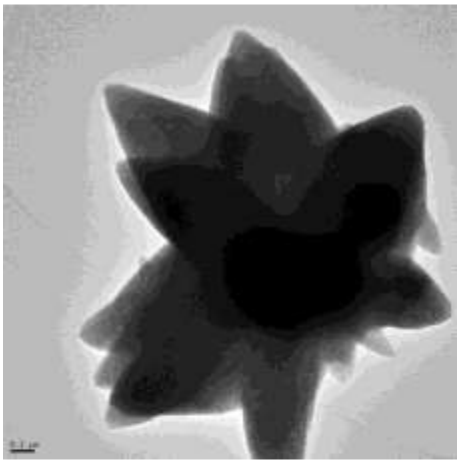

Figure S3. TEM BF overview image. No NPs are visible in bright field mode.

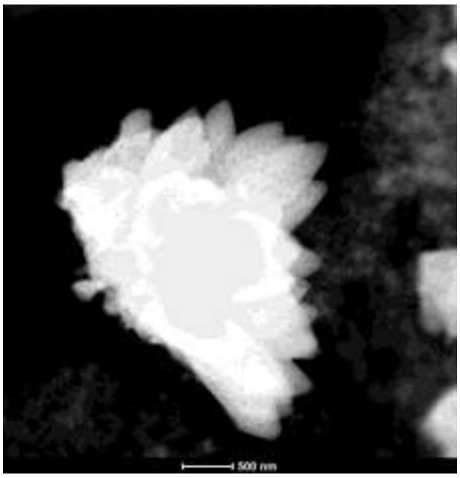

Figure S4. STEM-HAADF micrograph of a ZnO columnar structures. In low-magnification overview image no Ag/AgO NPs are visible.

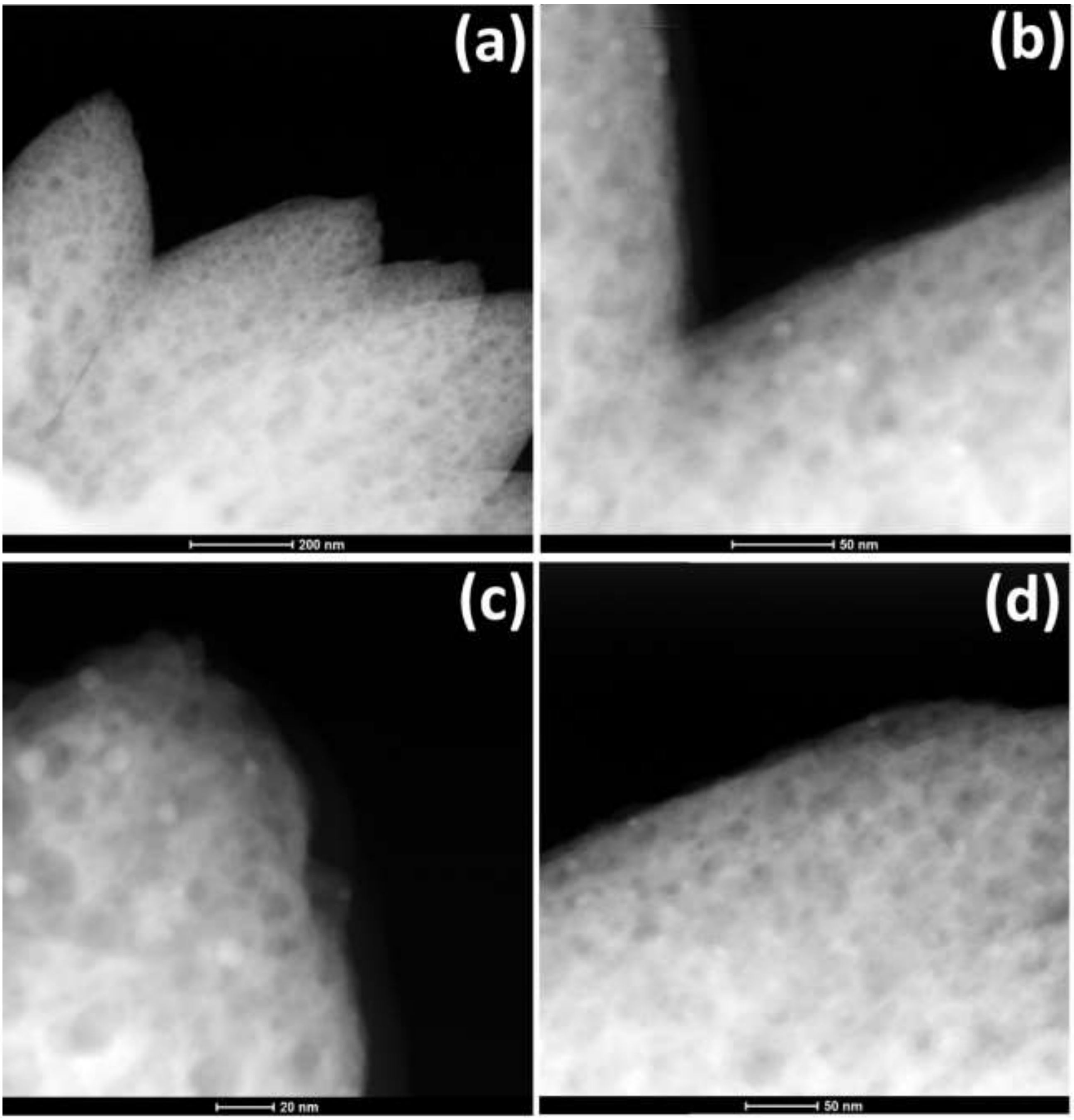

Figure S5. (a) STEM-HAADF micrograph at higher magnification of the ZnO microstructures. Some NPs are visible near the fringe of the ZnO microstructures. (b,c,d) STEM-HAADF micrograph at high magnification. Multiple Ag/AgO nanoparticles are visible as bright spots.

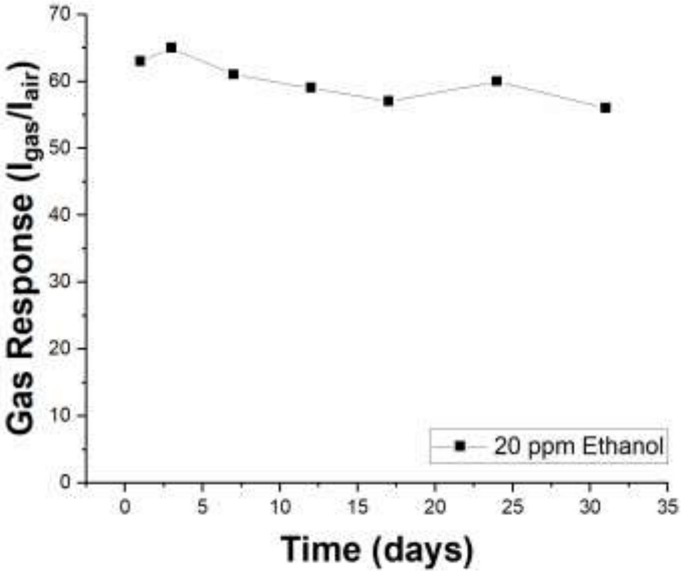

Figure S6. Long-term stability of Ag/ZnO:Fe nanostructured films to 20 ppm of ethanol at operating temperature of 300 ˚C.

Computational methods

A. Calculation details

We have employed the periodic plane-wave density functional theory (DFT) method within the Vienna a*b-initio* simulation package (VASP)[1-4] to simulate the adsorption of H_2, CH_4, CH_3CH_2OH and CH_3CHO to the modified ZnO $(10\bar{1}0)$ surface. We have used the Perdew, Burke and Ernzerhof (PBE) semilocal functional approximation for the exchange-correlation energy.[5] The projector augmented wave (PAW) method was used to model the atomic frozen core states and their interaction with the valence levels.[6, 7] The valence electrons comprised those in the 4*d*5*s* states for Fe and Ag, the 3*d*4*s* orbitals for Zn, the 2*s*2*p* levels for O and C as well as the 1*s* shell for H. The expansion of the Kohn-Sham (KS) valence states was calculated with a kinetic energy cut-off of 400 eV. The Brillouin zone electronic integrations were performed using a *Γ*-centred Monkhorst-Pack sampling grid[8] with a maximum separation of 0.7 $Å^{-1}$ between *k*-points, which is sufficient to describe the insulating properties of ZnO bulk.[9] This mesh density, which was double-checked with respect to the convergence of the total energy of the unit cell of ZnO bulk, corresponds to $4 \times 4 \times 2$ *k*-points. The ZnO $(10\bar{1}0)$ surfaces were modelled using the commensurate $1 \times 1 \times 1$ *k*-points mesh. The isolated molecules were simulated in a cell with broken symmetry, whose edges were approximately 5 times larger than the length of ethanol, the largest molecule considered in this study, sampling only the *Γ* point of the Brillouin zone. The electronic partial occupancies were determined using the Gaussian smearing method as ZnO was considered as an insulator. The width of the smearing was set at 0.05 eV, ensuring a negligible electronic entropy contribution to the free energy, which is the variational quantity in this form of finite temperature DFT.[10] Long-range dispersion interactions were modelled using the semi-empirical method of Grimme, with the Becke-Johnson damping [D3-(BJ)], which is essential to investigate the interaction of extended surfaces with molecular adsorbates, whilst avoiding unrealistic repulsive interatomic forces at short non-bonded distances.[11, 12] The optimization of the structures was conducted *via* the conjugate-gradients method, which stopped when the Hellmann-Feynman forces on all atoms were smaller than 0.01 $eV \cdot Å^{-1}$. We have used the Dudarev *et al.*[13] approach within the DFT+*U*[14] to improve the description of the localized and strongly correlated *d* states for the metal atoms. The values for the on-site Coulomb interaction term in this study were U_{eff} = 4.0 eV for Fe[14, 15] and 6.0 eV for both Ag[16] and Zn.[17] Spin-polarization was considered for all calculations as Fe is a ferromagnetic transition metal. These criteria allowed convergence of the total electronic energy within 10^{-4} eV per atom.

B. Surface models

The two ZnO $(10\bar{1}0)$ surface terminations were constructed by using METADISE[18] to cut the geometry optimized bulk. The surface slabs had a surface area of 98.574 Å^2 and contained 96 atoms, *i.e.* 48 formula units, and 8 atomic layers. The surface slabs are symmetric along the *z* axis and the stacking of the atomic layers in this direction is $(Zn_1{-}O_1){-}(Zn_2{-}O_2)$, with the ions inside brackets lying approximately within the same plane, which form the non-polar terminations A and B, presented in **Figure 5b** and **5c**, respectively. The four bottommost layers were frozen at the relaxed atomic bulk positions, to simulate the bulk phase, while the rest of the slab was allowed to relax, providing a single relaxed surface. We applied dipole corrections in the direction perpendicular to the surface,[19, 20] to account for the asymmetric introduction of the dopant and adsorbates. A vacuum gap of 20 Å was included above the surface in order to avoid interactions between the periodic slabs. The vacuum thickness as well as the total and relaxed number of surface layers were carefully tested until convergence to within 1 meV per atom was reached.

C. Calculation of surface energy and adsorption energy

We have based our analysis of the relative thermodynamic stabilities on the surface energies (γ) of the pristine terminations A and B of the ZnO $(10\bar{1}0)$ surface. As described in the section Surface models, our surface models for the two terminations are symmetric along the direction perpendicular to the slab. This condition allows us to treat separately the energies provided by the unrelaxed and relaxed halves of the simulation slabs, which is an approach widely used in the simulation of surfaces.[21-23] To obtain the contribution from the unrelaxed half of the cell, we calculate the surface energy (γ_u) from the energy of the slab with all atoms at their optimized bulk positions (E_u) as,

$$\gamma_u = \frac{E_u - n \cdot E_{bulk}}{2A} \tag{S1}$$

where n is the number of formula units contained in the surface cell, E_{bulk} is the energy of the bulk per formula unit and A is the surface area of one side of the slab.

Following geometry optimization of the uppermost half of the simulation cell, the surface energy of the relaxed side of the slab (γ_r) is calculated according to,

$$\gamma_r = \frac{E_r - n \cdot E_{bulk}}{A} - \gamma_u \tag{S2}$$

where E_r is the energy of the half-relaxed surface slab.

We also quantified the degree of relaxation (R) of each surface termination as a percentage of the surface energies for the unrelaxed and relaxed slabs, which was defined as

$$R = \frac{\gamma_u - \gamma_r}{\gamma_u} \cdot 100 \tag{S3}$$

The surface free energy (σ) after doping or adsorbing the clusters was obtained from the surface energy of the pristine surface as follows

$$\sigma = \gamma_r + \frac{E_{(AgO)_m/surf} - E_r - x \cdot E_{Fe} + x \cdot E_{Zn} - m \cdot E_{AgO}}{A} \tag{S4}$$

where $E_{(AgO)_m/surf}$ is the energy of the Fe-doped ZnO $(10\bar{1}0)$ surface decorated with the $(AgO)_m$ particle, x is the number of Fe dopants substituting Zn ions, $E_{Fe}(E_{Zn})$ is the energy of one atom in the bulk of *α*-Fe (*hcp* Zn), m is the number of AgO formula units and E_{AgO} is the energy per formula unit of AgO in the bulk.

The stability of the growing $(AgO)_m$ cluster was evaluated using the clustering energy (E_{clus}) per formula unit as

$$E_{clus} = \frac{E_{(AgO)_m/surf} - E_{surf} - m \cdot E_{AgO}}{m} \qquad \text{(S5)}$$

where E_{surf} is the energy of the Fe-doped ZnO $(10\bar{1}0)$ surface. A positive clustering energy indicates that the enlargement of the AgO cluster is favorable, while a negative value suggests that AgO prefers to wet the substrate.

The interaction of the Fe-doped ZnO $(10\bar{1}0)$ surface decorated with the $(AgO)_m$ nanoclusters and the molecular systems was measured using the adsorption energy (E_{ads}), which was derived as,

$$E_{ads} = E_{mol+(AgO)_m/surf} - E_{(AgO)_m/surf} - E_{mol} \qquad \text{(S6)}$$

where $E_{mol+(AgO)_m/surf}$ is the energy of the modified surface/adsorbate system and E_{mol} is the energy of the isolated adsorbate.

E. Simulation of the scanning tunnelling (STM) images

We have plotted the STM images for the modified ZnO $\left(10\bar{1}0\right)$ facets, which comprised the Fe dopant replacing Zn in the most favorable position and the $(AgO)_m$ cluster decorating the surface. To this end, we have used the most basic approximation of the Tersoff-Hamann formalism[24] as implemented in the HIVE-STM program,[25, 26] where the probe tip is treated as a point source. The tunneling current was simulated by integrating the local density of states (LDOS) charge density between the Fermi level and −2.0 eV, which is the energy that corresponds to the applied bias. The STM plots were mapped in the constant current mode, allowing also vertical displacements of the probe tip with respect to the surface to keep a constant charge density. Positive sampling bias represent a tunneling current moving from the STM tip towards the surface, while the contrary holds for the negative values.

F. Work function

The detection of ethanol vapours involves the electrocatalytic decomposition of the adsorbed molecules at the ZnO $\left(10\bar{1}0\right)$ surface. It has been shown that negatively charged oxygen atoms play a key role in this process and that the surface substrate acts as the source of electrons.[27-31] The introduction of metal dopants in various concentrations and lattice sites alongside transition metal oxide nanoclusters are known modifications to control the electron availability for heterogeneous catalysts, such as ZnO.[30, 32, 33] In this paper, we have used the work function (Φ) as a descriptor of the reducing character and reactivity of the pristine and modified ZnO $\left(10\bar{1}0\right)$ surface.[22, 26] The work function is defined as the energy required to remove the loosest held electron from the surface of a material to the vacuum. Theoretically, this is equivalent to measuring the thermodynamic work required to take out an electron from the Fermi level (E_F) into the electrostatic potential of the vacuum (V_V), which can be calculated as $\Phi = V_V - E_F$.

Table S1. Summary of the unit cell lattice (*a* and *c*) edges of the wurtzite ZnO reported from experiments (Ref. 34) and calculated.

	Experimental	**Calculated**
***a* (Å)**	**3.2501**	**3.2009**
***c* (Å)**	**5.2071**	**5.1327**

Table S2. Calculated surface energies before (γ_u) and after relaxation (γ_r) and the percentage of relaxation (*R*) for terminations *A* and *B* of the pristine ZnO $(10\bar{1}0)$ surface. The surface free energies (σ) are also reported for both terminations of the Fe-doped ZnO $(10\bar{1}0)$ surface. The work function (Φ) values are indicated for each surface.

Termination	**Doping site**	γ_u **(eV·Å^{-2})**	γ_r/σ **(eV·Å^{-2})**	Φ **(eV)**	***R***
A	pristine	0.220	0.190	5.40	13.81
	2-fold		0.140	2.37	
	4-fold		0.137	2.51	
B	pristine	0.104	0.084	5.80	19.49
	2-fold		0.084	2.36	
	4-fold		0.082	2.51	

Table S3. Calculated surface free energy (σ), work function (Φ) and clustering energy (E_{clus}) for the Fe-doped ZnO $(10\bar{1}0)$ surface decorated with the $(AgO)_m$ clusters. *m* represents the number of AgO formula units in the nanoparticle. The relative position of the $(AgO)_m$ nanoparticle with respect to the Fe dopant is also indicated.

m	**Relative position to Fe dopant**	**σ (eV·Å^{-2})**	**Φ (eV)**	**E_{clus} (eV)**
1	above	0.079	2.51	−0.335
	close	0.078	2.53	−0.338
	far	0.095	2.38	1.307
2	above	0.089	2.33	0.329
	close	0.083	2.46	0.050
	far	0.109	2.39	1.338
3	above	0.080	2.43	−0.068
	close	0.092	2.62	0.327
	far	0.105	2.98	0.753
4	above	0.098	2.81	0.396
	close	0.123	2.96	1.013
	far	0.117	3.08	0.867
5	above	0.099	3.03	0.333
	close	0.129	2.94	0.936
	far	0.133	3.02	1.013
6	above	0.111	3.14	0.478
	close	0.119	2.99	0.603
	far	0.137	3.08	0.900

Table S4. Adsorption energies (E_{ads}) of the H_2, CH_4, CH_3CHO and CH_3CH_2OH molecules for the three positions considered, i.e. above the cluster, at the cluster/surface interface and at the surface.

Molecule	***Position***	**E_{ads} *(eV)***
H_2	cluster	−0.154
	interface	−0.312
	surface	−0.308
CH_4	cluster	−0.134
	interface	−0.335
	surface	−0.326
CH_3CHO	cluster	−0.697
	interface	−0.667
	surface	−1.053
CH_3CH_2OH	cluster	−1.786
	interface	−0.998
	surface	−4.326

References

1. G. Kresse and J. Furthmüller, Efficient iterative schemes for ab initio total-energy calculations using a plane-wave basis set, *Phys. Rev. B*, 1996, **54**, 11169-11186.
2. G. Kresse and J. Furthmüller, Efficiency of ab-initio total energy calculations for metals and semiconductors using a plane-wave basis set, *Comput. Mater. Sci.*, 1996, **6**, 15-50.
3. G. Kresse and J. Hafner, Ab initio molecular dynamics for open-shell transition metals, *Phys. Rev. B*, 1993, **48**, 13115-13118.
4. G. Kresse and J. Hafner, Norm-conserving and ultrasoft pseudopotentials for first-row and transition elements, *J. Phys. Cond. Matter*, 1994, **6**, 8245.
5. J. P. Perdew, K. Burke and M. Ernzerhof, Generalized Gradient Approximation Made Simple, *Phys. Rev. Lett.*, 1996, **77**, 3865-3868.
6. P. E. Blöchl, Projector augmented-wave method, *Phys. Rev. B*, 1994, **50**, 17953-17979.
7. G. Kresse and D. Joubert, From ultrasoft pseudopotentials to the projector augmented-wave method, *Phys. Rev. B*, 1999, **59**, 1758.
8. H. J. Monkhorst and J. D. Pack, Special points for Brillouin-zone integrations, *Phys. Rev. B*, 1976, **13**, 5188-5192.
9. R. Escudero and R. Escamilla, Ferromagnetic behavior of high-purity ZnO nanoparticles, *Solid State Commun.*, 2011, **151**, 97-101.
10. N. D. Mermin, Thermal Properties of the Inhomogeneous Electron Gas, *Phys. Rev.*, 1965, **137**, A1441-A1443.
11. S. Grimme, J. Antony, S. Ehrlich and H. Krieg, A consistent and accurate ab initio parametrization of density functional dispersion correction (DFT-D) for the 94 elements H-Pu, *J. Chem. Phys.*, 2010, **132**, 154104.
12. S. Grimme, S. Ehrlich and L. Goerigk, Effect of the damping function in dispersion corrected density functional theory, *J. Comput. Chem.*, 2011, **32**, 1456-1465.
13. S. L. Dudarev, G. A. Botton, S. Y. Savrasov, C. J. Humphreys and A. P. Sutton, Electron-energy-loss spectra and the structural stability of nickel oxide: An LSDA+U study, *Phys. Rev. B*, 1998, **57**, 1505-1509.
14. V. I. Anisimov, M. A. Korotin, J. Zaanen and O. K. Andersen, Spin bags, polarons, and impurity potentials in $La_{2-x}Sr_xCuO_4$ from first principles, *Phys. Rev. Lett.*, 1992, **68**, 345-348.
15. D. Santos-Carballal, A. Roldan, R. Grau-Crespo and N. H. de Leeuw, First-principles study of the inversion thermodynamics and electronic structure of FeM_2X_4 (thio)spinels (M = Cr, Mn, Co, Ni; X = O, S), *Phys. Rev. B*, 2015, **91**, 195106.
16. J. P. Allen, D. O. Scanlon and G. W. Watson, Electronic structures of silver oxides, *Phys. Rev. B*, 2011, **84**, 115141.
17. V. Cretu, V. Postica, A. K. Mishra, M. Hoppe, I. Tiginyanu, Y. K. Mishra, L. Chow, N. H. de Leeuw, R. Adelung and O. Lupan, Synthesis, characterization and DFT studies of zinc-doped copper oxide nanocrystals for gas sensing applications, *J. Mater. Chem. A*, 2016, **4**, 6527-6539.
18. G. W. Watson, E. T. Kelsey, N. H. de Leeuw, D. J. Harris and S. C. Parker, Atomistic simulation of dislocations, surfaces and interfaces in MgO, *J. Chem. Soc. Faraday Trans.*, 1996, **92**, 433-438.
19. G. Makov and M. C. Payne, Periodic boundary conditions in ab initio calculations, *Phys. Rev. B*, 1995, **51**, 4014-4022.
20. J. Neugebauer and M. Scheffler, Adsorbate-substrate and adsorbate-adsorbate interactions of Na and K adlayers on Al(111), *Phys. Rev. B*, 1992, **46**, 16067-16080.
21. A. E. Shields, D. Santos-Carballal and N. H. de Leeuw, A density functional theory study of uranium-doped thoria and uranium adatoms on the major surfaces of thorium dioxide, *J. Nucl. Mater.*, 2016, **473**, 99-111.
22. D. Santos-Carballal, P. E. Ngoepe and N. H. de Leeuw, Ab initio investigation of the thermodynamics of cation distribution and of the electronic and magnetic structures in the $LiMn_2O_4$ spinel, *Phys. Rev. B*, 2018, **97**, 085126.
23. D. Santos-Carballal, A. Roldan, R. Grau-Crespo and N. H. de Leeuw, A DFT study of the structures, stabilities and redox behaviour of the major surfaces of magnetite Fe_3O_4, *Phys. Chem. Chem. Phys.*, 2014, **16**, 21082-21097.

24. J. Tersoff and D. R. Hamann, Theory of the scanning tunneling microscope, *Phys. Rev. B*, 1985, **31**, 805-813.
25. D. E. P. Vanpoucke and G. Brocks, Formation of Pt-induced Ge atomic nanowires on Pt/Ge(001): A density functional theory study, *Phys. Rev. B*, 2008, **77**, 241308.
26. M. G. Quesne, A. Roldan, N. H. de Leeuw and C. R. A. Catlow, Bulk and surface properties of metal carbides: implications for catalysis, *Phys. Chem. Chem. Phys.*, 2018, **20**, 6905-6916.
27. N. Bârsan and U. Weimar, Understanding the fundamental principles of metal oxide based gas sensors; the example of CO sensing with SnO_2 sensors in the presence of humidity, *J. Phys. Cond. Matter*, 2003, **15**, R813.
28. O. Lupan, V. Postica, J. Gröttrup, A. K. Mishra, N. H. de Leeuw, J. F. C. Carreira, J. Rodrigues, N. Ben Sedrine, M. R. Correia, T. Monteiro, V. Cretu, I. Tiginyanu, D. Smazna, Y. K. Mishra and R. Adelung, Hybridization of zinc oxide tetrapods for selective gas sensing applications, *ACS Appl. Mater. Interfaces*, 2017, **9**, 4084-4099.
29. V. Postica, J. Gröttrup, R. Adelung, O. Lupan, A. K. Mishra, N. H. de Leeuw, N. Ababii, J. F. C. Carreira, J. Rodrigues, N. B. Sedrine, M. R. Correia, T. Monteiro, V. Sontea and Y. K. Mishra, Multifunctional materials: A case study of the effects of metal doping on ZnO tetrapods with bismuth and tin oxides, *Adv. Funct. Mater.*, 2017, **27**, 1604676.
30. V. Postica, I. Hölken, V. Schneider, V. Kaidas, O. Polonskyi, V. Cretu, I. Tiginyanu, F. Faupel, R. Adelung and O. Lupan, Multifunctional device based on ZnO:Fe nanostructured films with enhanced UV and ultra-fast ethanol vapour sensing, *Mater. Sci. Semicond. Process.*, 2016, **49**, 20-33.
31. N. Yamazoe, New approaches for improving semiconductor gas sensors, *Sens. Actuators, B*, 1991, **5**, 7-19.
32. F. Paraguay D, M. Miki-Yoshida, J. Morales, J. Solis and W. Estrada L, Influence of Al, In, Cu, Fe and Sn dopants on the response of thin film ZnO gas sensor to ethanol vapour, *Thin Solid Films*, 2000, **373**, 137-140.
33. J. Qu, Y. Ge, B. Zu, Y. Li and X. Dou, Transition-Metal-Doped p-Type ZnO Nanoparticle-Based Sensory Array for Instant Discrimination of Explosive Vapors, *Small*, 2016, **12**, 1369-1377.
34. E. H. Kisi and M. M. Elcombe, *u* parameters for the wurtzite structure of ZnS and ZnO using powder neutron diffraction, *Acta Crystallogr. Sect. C Cryst. Struct. Commun.*, 1989, **45**, 1867-1870.

Author Contributions

V.P., A.V. and O.L. synthesized the Ag-functionalized ZnO:Fe nanomaterial. O.L. developed synthesis from chemical solution procedure SCS for ZnO. O.L., V.P., A.V. and F.S. adapted technological approach for material synthesis and integration/fabrication of the sensors. A.V., O.P., T.S. and F.F. developed functionalization procedure, set-up and realized all experiments and XPS analysis. P.V. and O.L. carried out the measurement of sensing properties of sensors based on such structures and analyzed data. J.S. and L.K. studied TEM. V.P., O.L., F.S., R.A., M.B. and P.V. analyzed the results, including Raman data and revised draft. N.H.L., D.S.C. and A.C.E. realized computational part. P.V., A.V., D.S.C., O.P and O.L. drafted the article. O.L., F.F., N.H.L., L.K. and R.A. study conception and design, final approval of the version to be published. All authors reviewed the manuscript.

Acknowledgements

Dr. Lupan acknowledges the Alexander von Humboldt Foundation for the research fellowship for experienced researchers 3-3MOL/1148833 STP at the Institute for Materials Science, Kiel University, Germany. This research was sponsored partially by the German Research Foundation (DFG) under the schemes FOR2093, SFB1261, A5, A6; KI1263/12-2 and by Project SFB859. This research was partly supported by the STCU within the Grant 6229. We acknowledge the Engineering and Physical Sciences Research Council (EPSRC grant EP/K009567) for funding. Via our membership of the UK's HEC Materials Chemistry Consortium, which is funded by EPSRC (EP/L000202), this work used the ARCHER UK National Supercomputing Service (http://www.archer.ac.uk). This work was performed using the computational facilities of the Advanced Research Computing @ Cardiff (ARCCA) Division, Cardiff University. The authors also acknowledge the use of HPC Wales, Supercomputing Wales and associated support services in the completion of this work. All data created during this research is openly available from the Cardiff University's Research Portal at http://doi.org/10.17035/d.2018.0054411689